 doi:10.20944/preprints202206.0199.v1

Article

Disruption of a conservative motif in the C-terminal loop of the KCNQ1 channel causes LQT syndrome

Maria Karlova[1], Denis V. Abramochkin[1], Ksenia B. Pustovit[1], Tatiana Nesterova[2,3], Valery Novoseletsky[1,4], Gildas Loussouarn[5], Elena Zaklyazminskaya[6] and Olga S. Sokolova[1,4]*

[1] Lomonosov Moscow State University, Faculty of Biology, Moscow, 119234, Russia; mkarlova@yandex.ru (M.K.); abram340@mail.ru (D.V.A.); sokolova@mail.bio.msu.ru (O.S.S); k_pustovit@mail.ru (K.B.P.); valery.novoseletsky@yandex.ru (V.N.)
[2] Institute of Immunology and Physiology, Ural Branch of Russian Academy of Sciences, Ekaterinburg, 620049, Russia. (T.N.)
[3] Institute of Natural Sciences and Mathematics, Ural Federal University, Ekaterinburg, 620075, Russia.
[4] Shenzhen MSU-BIT University, Biology department, Shenzhen, 517182, China.
[5] Nantes Université, CNRS, INSERM, l'institut du thorax, F-44000 Nantes, France; gildas.loussouarn@univ-nantes.fr (G.L.)
[6] Russian Scientific Center for Surgery named after B.V.Petrovsky, Moscow, 119991, Russia; zhelene@mail.ru (E.Z.)

* Correspondence: sokolova@mail.bio.msu.ru

Abstract: We identified a single nucleotide variation (SNV) (c.1264A>G) in the KCNQ1 gene in a 5-year-old boy who presented with a prolonged QT interval. His elder brother and mother, but not sister and father, also had this mutation. This missense mutation leads to a p.Lys422Glu (K422E) substitution in the Kv7.1 protein, never mentioned before. We inserted this substitution in an expression plasmid containing Kv7.1 cDNA and studied the electrophysiological characteristics of the mutated channel expressed in CHO-K1 using the whole-cell configuration of the patch-clamp technique. Expression of the mutant Kv7.1 channel in both homo- and heterozygous conditions, in the presence of auxiliary subunit KCNE1, results in a significant decrease in tail current densities compared to the expression of wild-type (WT) Kv7.1 and KCNE1. This study also indicates that K422E point mutation causes a dominant negative effect. The mutation was not associated with a trafficking defect, the mutant channel protein was confirmed to localize at the cell membrane. This mutation disrupts the poly-Lys strip in the proximal part of the highly conserved cytoplasmic A-B linker of Kv7.1, which was not shown before to be crucial for channel functioning.

Keywords: KCNQ1; Kv7.1; I_{Ks}; patch-clamp; inherited channelopathy; LQTS

1. Introduction

Potassium currents I_{Ks}, I_{Kr}, I_{t0}, I_{K1}, I_{Ss}, I_{K2P} all contribute to repolarization in cardiomyocytes in normal and failing hearts [1]. Mutations in genes encoding the alpha and beta subunits of the potassium channels conducting these currents lead to several arrhythmic disorders such as Long QT syndrome (LQTS), Short QT syndrome (SQTS), familial atrial fibrillation (FAF), Brugada syndrome (BrS), early repolarization syndrome (ERS), and can also be found in cardiac sudden death (SCD) victims (OMIM). Loss-of-function mutations (LoF) usually lead to LQTS [2-4], whereas gain-of-function (GoF) mutations have a more variable appearance (SQTS, BrS, ERD, FAF) [4, 5]. Presumably, the clinical phenotype and the changes in ECG in patients with mutations in these genes correlate with ion permeability defects. On the other hand, there are many mixed and overlapping phenotypes, resulting from complex molecular pathways of channel dysfunction. Modern new generation sequencing (NGS) technologies provide a unique opportunity to simultaneously test

Preprints (www.preprints.org) | NOT PEER-REVIEWED | Posted: 14 June 2022 doi:10.20944/preprints202206.0199.v1

multiple genes in patients with suspected channelopathies and to identify the genetic cause of the disease [6]. But the large volume of performed genetic testing reveals many rare/unique genetic variants of unknown clinical significance. The correct interpretation of these genetic findings is crucial for correct genetic counseling and clinical care including the selection of the best choice of anti-arrhythmic treatment, SCD risk estimation and decision making about anti-arrhythmic device implantation. Hence, functional studies of newly discovered variants are critical to classify the variant as pathogenic or non-pathogenic.

KCNQ1 is a gene encoding the alpha subunit of the voltage-gated cardiac K^+ channel complex, Kv7.1 (also named KCNQ1). This subunit assembles with the auxiliary beta subunit KCNE1 to form functional channel and generate the slowly activating delayed rectifier K^+ current, I_{Ks}. This current plays an important role in the repolarization of cardiac cells and the maintenance of the normal duration of cardiac action potentials. Mutations in the KCNQ1 gene are most common in patients with LQTS, the most common cardiac channelopathy [6]. Congenital LQTS is characterized by asynchronous and delayed ventricular repolarization, is predisposed to a high risk of ventricular tachyarrhythmias and sudden cardiac death [7].

The Kv7.1 ion channel family lacks the T1 tetramerization domain, and does not associate with the cytoplasmic beta subunit, as in *Shaker* family channels [8, 9]. Rather, it has a large intracellular C-terminal domain, ranging from 320 to 500 residues in size, bound constitutively to calmodulin (CaM) [10]. The C-terminal cytoplasmic domain is responsible for channel tetramerization, proper channel trafficking, and maintaining of biophysical properties [11]. It comprises of A, B, C, and D domains, interconnected by A-B and B-C linkers [12]. A and B helices mediate binding to CaM [13]. The A-B linker is presumably unstructured, and this highly conserved loop has been predicted to be susceptible to proteolysis. Previous electrophysiological experiments demonstrated that the A-B linker is not crucial for the correct functioning of Kv7 channels [14, 15] and, thus, it has been removed in various structural studies [13, 16]. Recently, the structure of Kv7.1 with bound auxiliary subunit KCNE3, phospholipid phosphatidylinositol (4-5) bisphosphate (PIP_2), and CaM has been solved by cryo-EM [10], which revealed conformational changes in CaM and the cytoplasmic A subunit upon binding of PIP_2.

Here, we identified a new single nucleotide variation (SNV) c.1264A>G (NM_000218.2) in a patient with LQTS. This variant is located in an A-B unstructured linker. The aim of this study was to perform a detailed biochemical and electrophysiological characterization of the Kv7.1-K422E mutant channel, and to assess the possible role of this LoF mutation in QT prolongation.

2. Results

2.1 Clinical Case

Asymptomatic QTc prolongation (QTc 480 ms resting, and up to 587 ms in ortho probe) was registered in a 5 y.o. male proband from a consanguineous family of Daghestani origin during a routine ECG screening (Figure 1a). Familial history was unremarkable, no SCD event or syncope in the family were disclosed by proband's parents. Further clinical evaluation detected asymptomatic QTc prolongation in proband's mother (31 y.o., QTc 489-495 ms) and his 13 y.o. brother (QTc 478-485 ms). Proband's sister (8 y.o.) and proband's father (41 y.o.) had QTc within normal range (419 ms and 424 ms, respectively). Targeted gene panel testing revealed a rare non-characterized genetic variant c.1264A>G (p.Lys422Glu) in the KCNQ1 gene in the proband's DNA (Figure 1b). The variant was assessed as a variant of unknown significance (VUS) according to ACMG2015 criteria. Familial genetic investigation detected two more carriers of this variant (mother and brother), both with QTc prolongation (Figure 1).

Preprints (www.preprints.org) | NOT PEER-REVIEWED | Posted: 14 June 2022 doi:10.20944/preprints202206.0199.v1

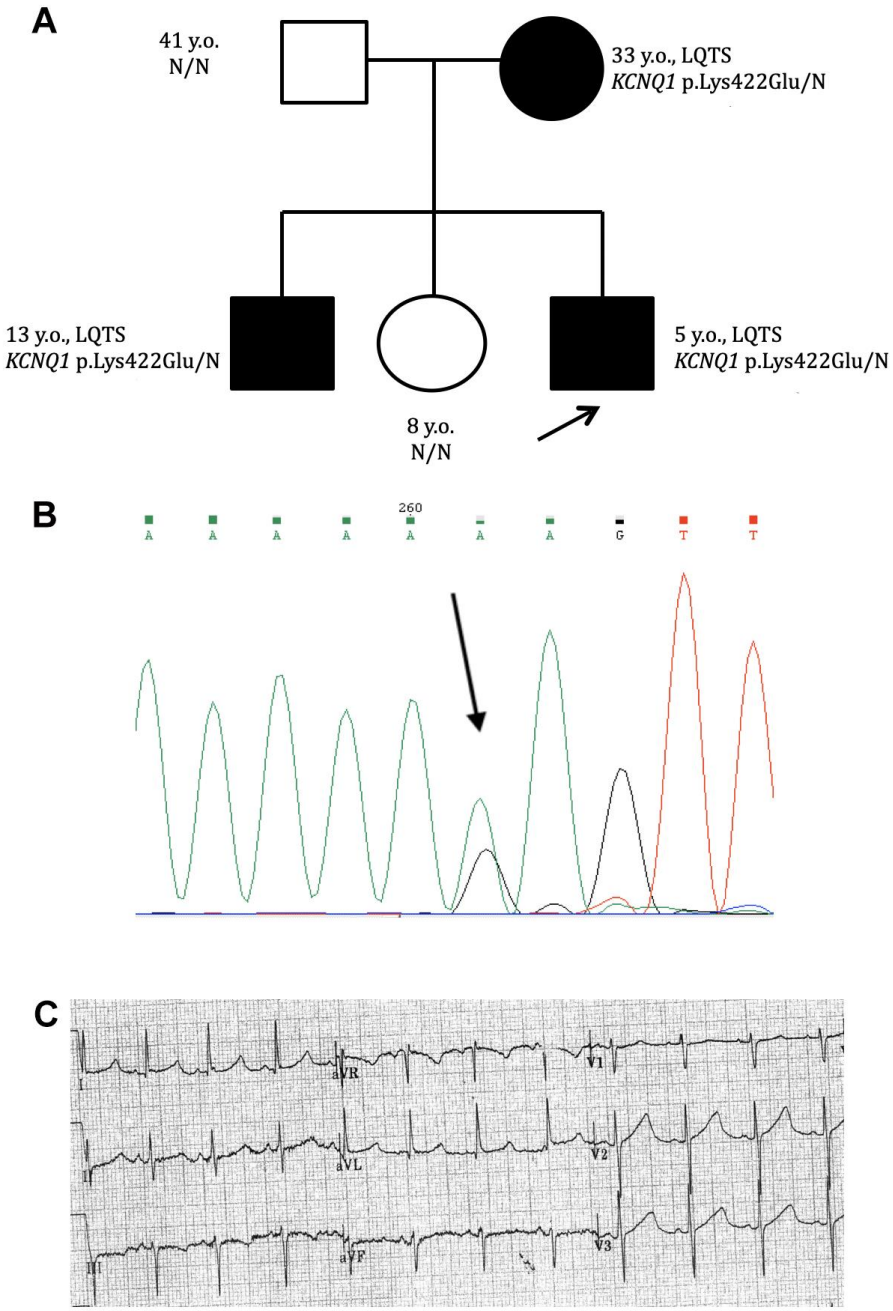

Figure 1. (**a**) Pedigree of family with genetic variant c.1264A>G (K422E) in the KCNQ1 gene. Family members with QTc prolongation - closed symbols, healthy individuals - open symbols. Arrow - proband. (**b**) Confirmation of the heterozygous c.1264A>G variant in the KCNQ1 gene by Sanger sequencing. Arrow - a.a. substitution. (**c**) Fragment of the proband's ECG (5 y.o., male, standing). Sinus rhythm, HR, 102 bpm, PQ, 142 ms, QTc, 570- 587 ms.

2.2 Expression and Subcellular localization of WT and mutant Kv7.1 channels

To check if the point mutation affects the Kv7.1 channel expression, the protein expression level was analyzed by immunoblot. The point mutation was introduced into the KCNQ1 cDNA, cloned into the appropriate vector and expressed in CHO-K1 cells. An equal number of cells (50,000) were resuspended in PBS (10 ul) and loaded onto SDS-PAAG. Alpha-tubulin was used as loading control. Immunoblot analysis (Figure 2a) showed no differences in the Kv7.1 protein expression level in whole-cell lysates of CHO-K1 cells expressing WT or the K422E mutant (n = 3 blots from three transfections).

Preprints (www.preprints.org) | NOT PEER-REVIEWED | Posted: 14 June 2022 doi:10.20944/preprints202206.0199.v1

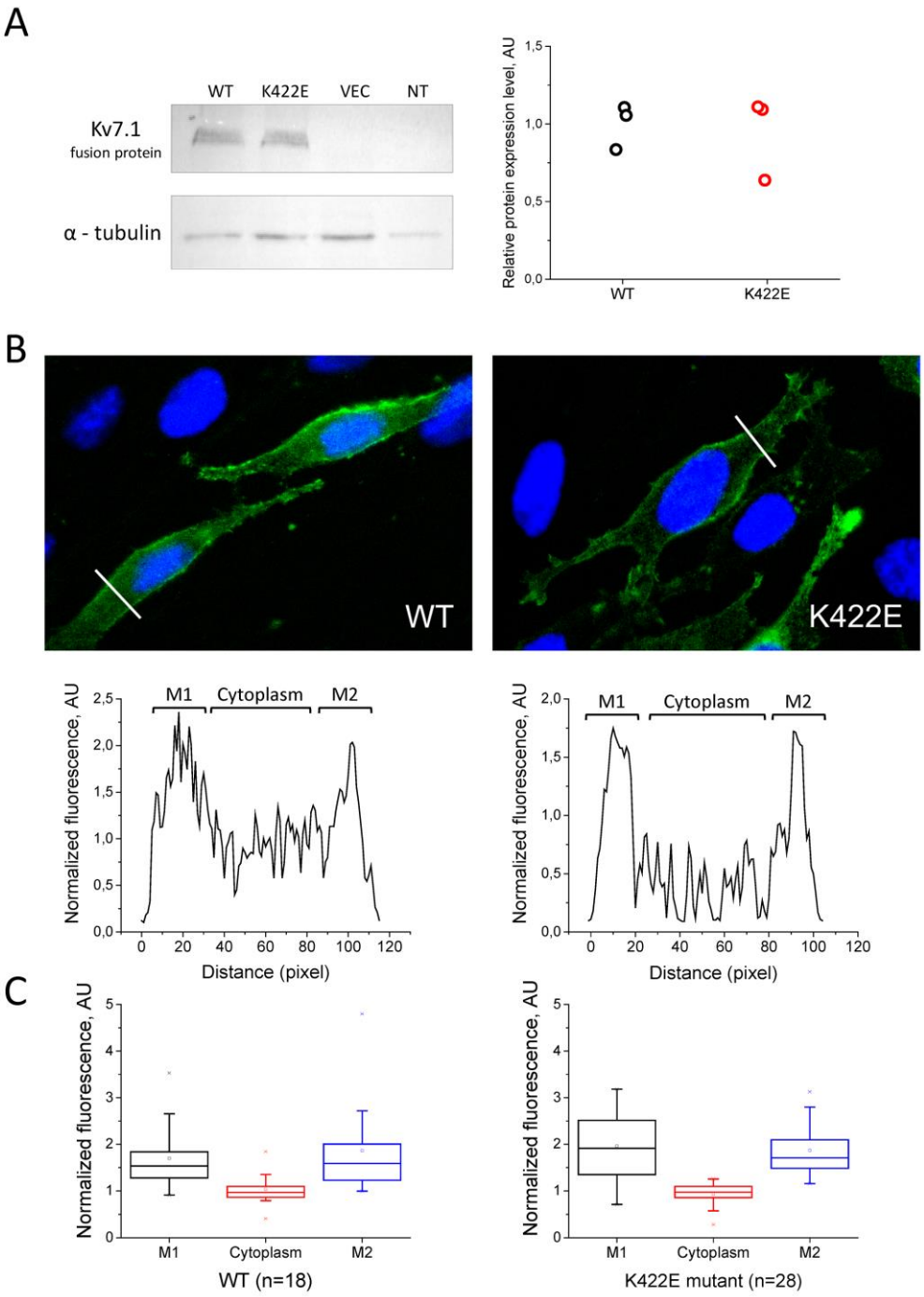

Figure 2. (**a**) Immunoblot analysis of Kv7.1 expression in whole-cell lysates of CHO-K1 cells. WT – cells, transfected with control Kv7.1 protein, K422E – cells, transfected with Kv7.1 protein with K422E mutation, VEC – cells, transfected with an empty vector, NT – non-transfected cells. Primary antibodies against V5-tag and alpha-tubulin. (n = 3 blots from three transfections). (**b**) Immunofluorescent staining of CHO-K1 cells expressing the recombinant Kv7.1 protein: wild-type (top left) and mutant (top right). Primary antibody against V5-tag, secondary antibody conjugated to alexa-488 dye (green channel). Bottom – intensity of green signal across the cell (along the white lines in the images in the top row) with the two peaks corresponding to cell plasma membrane. (**c**) Statistical analysis of the surface plots of Kv7.1 fluorescence intensity signal, mean ±S.E. fluorescence of Kv7.1 (WT, 18 cells, left and K422E mutant, 28 cells, right) normalized to the average cell fluorescence intensity signal.

Preprints (www.preprints.org) | NOT PEER-REVIEWED | Posted: 14 June 2022 doi:10.20944/preprints202206.0199.v1

To determine the effect of the mutation on the membrane expression of the Kv7.1 channel, fluorescent microscopy of CHO-K1 cells expressing Kv7.1-WT and Kv7.1-K422E subunits was performed. Analysis of the signal intensity across the cell (Figure 2b, below) confirmed membrane expression for both WT and mutant channels. As shown in plots on Figure 2c, both channel proteins showed substantial membrane localization. These data indicate that the K422E mutation does not disturb expression and membrane trafficking of the mutant Kv7.1 protein.

2.3 Electrophysiological properties of WT and K422E channel complexes

A typical slow delayed rectifier K+ current (IKs) with slow activation and without any visible inactivation was elicited in transfected CHO-K1 cells by a 6-s depolarizing pulse from the holding potential of -80 mV to the potentials from -20 to +80 mV with 20 mV steps (Figure 3a). The mutant current was significantly downregulated for both WT/K422E (Figure 3b) and K422E/K422E groups (Figure 3c).

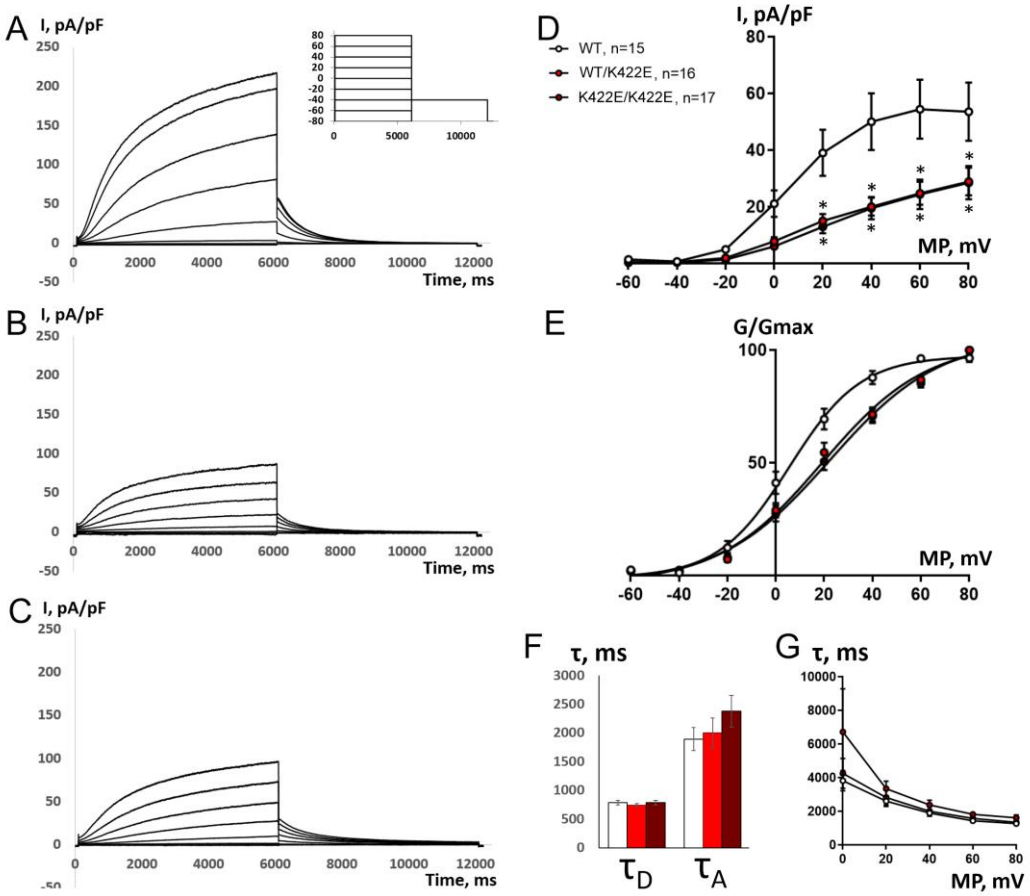

Figure 3. Electrophysiological properties of IKs current in transfected CHO-K1 cells. (**a-c**) Original recordings of the current from 3 representative cells transfected with plasmid containing KCNE1 cDNA and either the WT Kv7.1 cDNA (**a**, n=4), or the same cDNA with introduced K422E mutation (**b**, n=3) or 1:1 combination of these two plasmids (**c**, n=3). The current was elicited by the 2-step square-pulse depolarization, shown in the inset, from the holding potential of -80 mV. The second step to -40 mV was used to analyze the outward tail current. (**d-g**) Comparison of the main parameters of IKs recorded from cells transfected with plasmid containing the WT Kv7.1 cDNA (n=15), the same cDNA with introduced K422E mutation, K422E/K422E (n=17) or 1:1 combination of these two plasmids (WT/K422E, n=16). (**d**) I-V curves of peak tail IKs current in 3 groups of cells. * – significant difference from WT group, $p<0.05$, two-way ANOVA with Tukey's post-hoc test. (**e**) activation curves of IKs in 3 groups of cells. (**f**) comparison of tail current deactivation kinetics (τD) after +40 mV depolarization in 3 groups of cells and IKs activation kinetics at depolarizing step to +40 mV (τA). (**g**) comparison of IKs activation kinetics in three groups of cells at potentials ranging from 0 to +80 mV.

Preprints (www.preprints.org) | NOT PEER-REVIEWED | Posted: 14 June 2022 doi:10.20944/preprints202206.0199.v1

To determine the voltage dependence of activation, a series of depolarizing pulses were applied during 6 sec, ranging from -60 to +80 mV, in 20 mV steps, for WT/WT, WT/K422E, and K422E/K422E groups (Figure 3a-c). Tail current densities measured at -40 mV were plotted as a function of the prepulse potential (Figure 3d). In the WT group, IKs current activation curve was almost saturated at +60 and +80 mV, while in both K422E/K422E and WT/K422E groups, saturation was still not reached. Both WT/K422E and K422E/K422E showed a rightward shift of the activation curve (Figure 3e) indicated by a more positive V0.5 in comparison with the WT group (Table 1, supplement). The slope factors were significantly larger in both WT/K422E and K422E/K422E groups in comparison with the WT group (Table 1, supplement). However, no significant differences of V0.5 and slope factor were found between K422E/K422E and WT/K422E. The superposition of K422E/K422E and WT/K422E I/V curves and activation curves shows that K422E mutation exerts a dominant negative effect on WT subunit, otherwise the WT/K422E activation curve would have been situated between the WT/WT and the K422E/K422E activation curve. At +60 mV, both the activation kinetics (τA) and tail current deactivation kinetics (τD) did not show any difference between WT, K422E/K422E, and WT/K422E groups (Figure 3f).

2.4 Modeling of the influence of the K422E mutation on simulated human ventricular AP

Next, to evaluate the impact of Kv7.1 on the LoF, we performed mathematical simulations. To assess the effect of the K422E mutation on the AP waveform we used the ionic model of human ventricular AP (epicardial version) TP2006 [17]. The model includes parameters of all major ionic currents of a human ventricular myocyte (see Methods). Since the model was successfully used in numerous studies [18], it could be considered as one of the most reliable models for electrical activity of the non-ischemic human ventricular myocyte.

The comparison of simulated APs and related AP-induced IKs current traces is shown in Figure S1. The K422E mutation leads to marked AP prolongation at 50 and 90% repolarization levels without substantial changes in AP amplitude and resting membrane potential (Table 2, supplement). The AP-induced IKs traces are characterized by slower activation and a lesser maximal value (Figure S1). Thereby, the results of our simulation study allow to propose the slowing of repolarization induced by K422E mutation in human ventricular cardiomyocytes, leading to the prolongation of the QT interval and the provocation of ventricular tachyarrhythmias.

3. Disscussion

3.1 K422E mutation analysis

In this study, a toddler LQTS proband was found to have SNV c.1264A>G in the KCNQ1 gene, resulting in p.Lys422Glu (K422E) amino acid substitution at the cytoplasmic C-terminus tail of the alpha-subunit of the IKs channel. This unique genetic variation has not been registered or characterized earlier. Two different allelic variants, p.Lys422Arg (K422R, single allele in gnomAD genomes, total MAF 0.00003191) and p.Lys422Thr (K422T, two alleles in gnomAD exomes, total MAF 0.000007917), were registered in gnomAD (https://gnomad.broadinstitute.org/). The variant found within this study was classified as a variant of unknown significance (VUS, Class III) and at the moment of detection could not be used for diagnosis confirmation. Segregation analysis revealed this SNV in the two additional family members (older brother and mother) that also had asymptomatic QTc prolongation (Figure 1a). The sister and father had no QTc prolongation, nor carried this variant in their DNA.

To clarify the relationship between the K422E variant and the clinical phenotype, we inserted this substitution into the channel sequence and performed a detailed experimental investigation. The influence of this variant on the total expression level or on membrane distribution was ruled out by performing immunofluorescent analyses. Electrophysiological experiments showed that the K422E-Kv7.1 mutation results in the decrease of the K+ current and the alteration of channel activity (Figure 3).

 doi:10.20944/preprints202206.0199.v1

We demonstrate that the exogenously expressed Kv7.1-K422E alpha subunit is sufficient for the disruption of Kv7.1 channel function (Figure 3), even when co-expressed with the WT form of the protein, suggesting that K422E is a dominant negative mutation. Thus, we obtained experimental evidence that this variant significantly alters channel permeability and can be characterized as a LoF mutation.

Numerous studies of C-terminal mutations in the KCNQ1 gene have previously shown that they often cause trafficking defects [19-21]. The mutation described here was not associated with a trafficking defect, since the mutant channel protein was detected at the cell membrane, similarly to the WT channel (Figure 2b, c).

According to prior studies [22], the majority of mutations (70%) that lead to LQTS are located in the pore region and in transmembrane domains S5 and S6 that are immediately adjacent to the pore, the rest (30%) – in the N- and C-termini. The pore region mutations appeared to result in a more severe phenotype. On the contrary, patients with the K422E mutation located at the C-terminus showed a mildly affected phenotype.

Thus, we obtained experimental evidence that this variant significantly alters channel permeability and can be characterized as a LoF mutation. This is a classical mechanism of KCNQ1-mutations leading to prolonged repolarization, which we clinically observe as a QTc prolongation on resting ECG. So, functional data are in accordance with the clinical presentation (LQTS) in the family, and we can re-classify this variant as a "likely pathogenic" (Class IV) with PS3 (experimental *in vitro* evidence), PM2 (rarity in population), and PP3 (9 *in silico* predictors are in favor of pathogenicity) ACMG2015 criteria.

3.2 Proposed Mechanisms of Functional Loss

Here, we identified the single positive amino acid substitution to a negatively charged one, which lead to a dramatic shift in I-V curves towards positive potentials (Figure 3). This shift suggests the presence of defective voltage sensing. A model that describes the voltage sensing of the Kv7.1 channel is a ligand/receptor model suggesting a loose coupling between the voltage sensors and the pore in Kv7.1 [23]: when the voltage sensors are resting, the S4-S5 linker binds to the S6 C-terminus as a ligand to its receptor, stabilizing the pore in a closed conformation; during the activation, S4 drags the S4-S5 linker away from S6, releasing the pore. This model agrees with the experimental data not only for Kv7.1, but also cardiac Kv11.1 and neuronal Kv10.2 channels [24-26]. In these experiments, designed peptides that share a similar amino acid sequence with the S4-S5 linker (the ligand) of Kv7.1, Kv10.2, Kv11.1 channels were co-expressed with the full-length channel, which resulted in a reduction of the voltage-dependent potassium current. One possibility would be that the unstructured A-B linker in the Kv7.1 channel, which comprises of 120 residues, could possibly span the distance of up to 35 nm in an extended conformation, sufficient to traverse the length between the voltage sensor and the cytoplasmic C-terminus of the channel.

Introducing negatively charged Glu into position 422 apparently disrupts a conserved poly-Lys strip (Figure 4a, b) and may lead to the alteration of electrostatic interactions with other regions of the channel. This hypothesis agrees well with the fact that the substitution of Lys at the same position to the polar Thr residue did not affect the currents in the mutant channels, as compared to the WT [27].

Preprints (www.preprints.org) | NOT PEER-REVIEWED | Posted: 14 June 2022 doi:10.20944/preprints202206.0199.v1

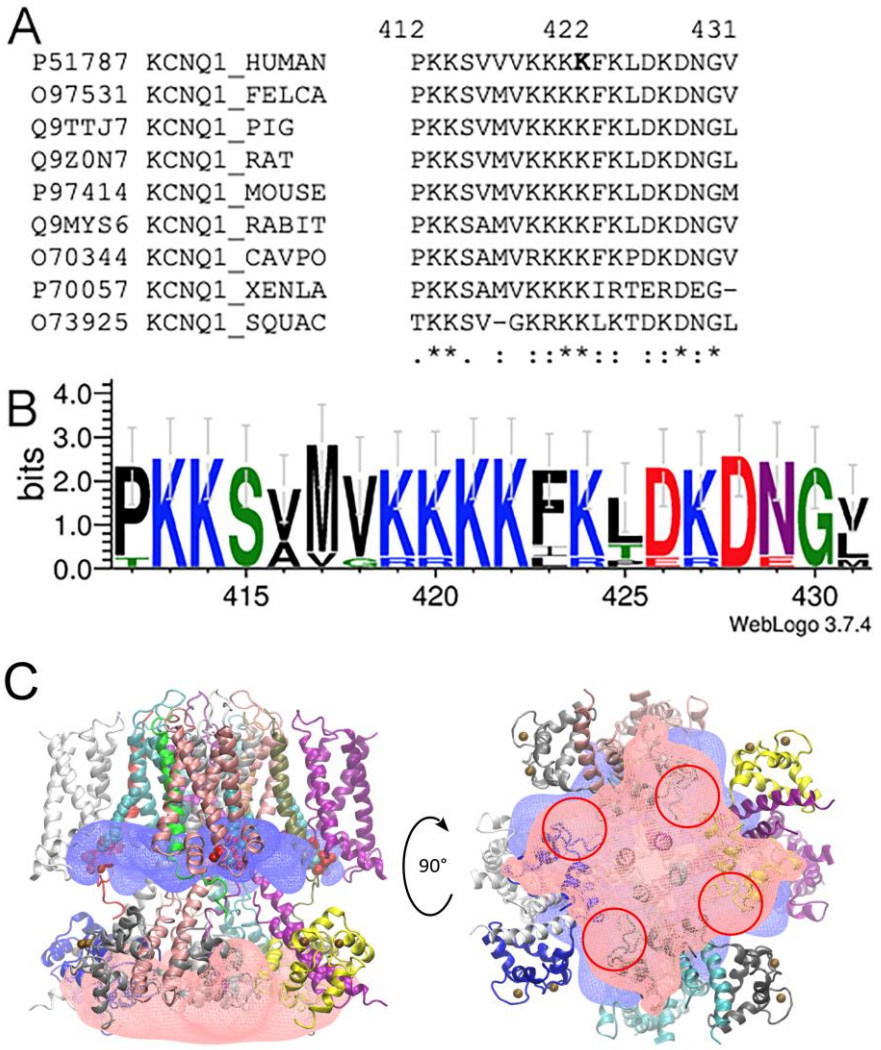

Figure 4. (**a**) Multiple sequence alignment for the 412-431 fragments of the human Kv7.1 and corresponding fragments of their relative sequences. (**b**) Sequence logo for the fragment of an alignment of several Kv7.1 sequences. The height of each residue is proportional to its frequency, while the height of the overall stack of residues is inversely proportional to Shannon entropy. (**c**) Electrostatic potential maps showing positive (blue) and negative (red) potential near the Kv7.1-KCNE3-CaM-PIP_2 complex. Blue and red electrostatic potential maps correspond to +400 kT/e and -400 kT/e, respectively. Protein chains are colored according to their IDs. Four PIP_2 molecules shown in space-filling representation. Eight Ca^{2+} ions are shown with brown spheres. Red circles correspond to the regions with the highest values of negative potential.

In order to have more insights on the possible pathophysiological mechanism, we modeled the electrostatic potentials in the cytoplasmic area of the Kv7 channel (Figure 4c) using the cryo-EM 3D reconstruction of a partially truncated (N- and C-termini were removed) Kv7.1 channel with bound CaM, auxiliary subunit KCNE3 and PIP_2 lipids [10] (pdb id 6v01).

Post translational modifications (PTM) of CaM were introduced according to Uniprot (https://www.uniprot.org/uniprot/P0DP23#ptm_processing), which lead to the net negative charges of -19 for every subunit of the cytoplasmic domain (+3 for fragment 355-390 and +10 for fragment 500-570 of Kv7.1, and -32 for CaM with PTM), which are partially neutralized by 8 Ca^{2+} ions (two of four possible for every CaM molecule). High values of the net charge generate substantial negative potential in the cytoplasmic domain and we propose that this region (especially CaM molecules) could be a target for KKKKFK motif binding. The most negative regions of the potential are located in the vicinity of residues

 doi:10.20944/preprints202206.0199.v1

100 and 135, which belong to Ca^{2+}-binding motifs, but in the current structure (pdb id 6v01) ions were absent in these sites. On the other hand, these regions are at the interface between CaM molecules (Figure 4c) formed with residues D79, D81, E83, E84, E85, and E88 of one molecule and residues D96, phosphorylated Y100, phosphorylated S102, D132, D134, phosphorylated Y139, E140, E141 of the other. We suggest that a positively charged KKKKFK motif could bind to this interface and stabilize it. Mutation K422E substantially decreases the charge of this motif and, hence, its ability to stabilize the CaM-CaM interface, which may lead to a repulsion of channel subunits in the cytoplasmic domain and to the disruption of channel function. More experiments are needed to establish these interactions.

4. Materials and Methods

Clinical and Genetic Evaluation

Clinical and genetic evaluation was performed in accordance with the principles of the Declaration of Helsinki, and with the written informed consent of adult family members. Instrumental examination included general examination, collection of personal and family history, general biochemical blood tests, resting and standing ECG 24-hr Holter ECG monitoring, and echocardiography (EchoCG). Genetic study for proband was performed on DNA samples isolated from venous blood leukocytes, according to standard protocol. NGS of the target panel of 11 genes (KCNQ1, KCNH2, KCNJ2, KCNE1, KCNE2, SCN5A, SCN1B-4B, and SNTA1) was performed based on the Ion Torrent PGM platform using the Ion AmpliSeq™ Exome Kit (Thermo Fisher Scientific, Waltham, MA, USA). Primary data processing was performed using Ion Proton Software (Thermo Fisher Scientific, Waltham, MA, USA); alignment with the hg19 version DNA reference sequence was performed using the BWA 0.7.9 software. The pathogenicity of the identified variants was assessed using the ACMG2015 pathogenicity criteria [28]. All rare (MAF< 0.01%) variants found by NGS were confirmed by capillary bidirectional Sanger re-sequencing on the ABI 3730XL DNA Analyzer (Thermo Fisher Scientific) according to manufacturer protocol. Cascade genetic testing for the family members was also performed using the same instrument.

Plasmids

For Kv7.1 protein expression, two constructs were used. The first one – pcDNA6-V5-HisA/hKCNE1-hKCNQ1 – contains the human KCNE1 auxiliary subunit fused to the human Kv7.1 alpha-subunit, inserted in frame with V5 and 6xHis tags in a pcDNA6-V5-HisA vector (Invitrogen). The second – plasmid pIRES2-EGFP/hKCNQ1-1D4 – contains the human Kv7.1 alpha-subunit cDNA augmented with a 1D4-tag on the C-terminus of the polypeptide chain inserted in the pIRES2-EGFP vector (Clontech). Plasmid construction was described earlier [29]. These plasmids were used as wild-type (WT) control and for mutagenesis. For electrophysiological experiments the pIRES2-EGFP/hKCNQ1-1D4 (WT and K422E mutant) plasmids were used. For fluorescent microscopy, the pcDNA6-V5-HisA/hKCNE1-hKCNQ1 (WT and K422E mutant) plasmids were used, since the eGFP expression of the pIRES-EGFP vector interferes with the immunofluorescent staining. The construction of the pRC-KCNE1 plasmid encoding the KCNE1 auxiliary subunit was described elsewhere [30].

Introduction of a point mutation into a channel sequence

Mutations were introduced into plasmids pcDNA6-V5-HisA/hKCNE1-hKCNQ1 and pIRES2-EGFP/hKCNQ1-1D4 using site-directed mutagenesis. Single-point substitution was added to a forward primer. Non-overlapping reverse primers were used according to the polymerase manufacturer recommendations. Oligonucleotide AAAGAAAAAA-GAGTTCAAGCTGGAC was used as a forward primer and oligonucleotide ACCAC-CACAGACTTCTTG as a reverse primer. PCR was conducted with Q5 High-Fidelity polymerase in the presence of a GC-enhancer (Neb, USA). Mutagenesis was verified by sequencing.

Preprints (www.preprints.org) | NOT PEER-REVIEWED | Posted: 14 June 2022 doi:10.20944/preprints202206.0199.v1

Cell Culture and transfection

Cells were incubated in DMEM/F12 medium (Gibco, Thermo Fisher Scientific, USA) with 10% fetal bovine serum (HyClone, USA), 2 mM glutamine, 100 U/ml penicillin, 100 mg/ml streptomycin (Thermo Fisher Scientific, USA) in a CO2 incubator at 37ºC.

A mixture of 0.5 μg pIRES2-EGFP/hKCNQ1-1D4 with cDNA encoding the Kv7.1 alpha-subunit, 0.5 μg pRC-KCNE1 with cDNA for the KCNE1 subunit and 0.1 μg pMAX with cDNA for the green fluorescent protein (GFP) were co-transfected into CHO-K1 cells growing on round 35 mm Petri dishes, using Lipofectamine® LTX with Plus™ Reagent (Thermo Fisher Scientific, USA). While the control group of cells (WT) was transfected with plasmid containing wild-type alpha-subunit cDNA, the "homozygous" experimental group (K422E/ K422E) was transfected with plasmid containing mutant cDNA. The "heterozygous" experimental group (WT/K422E) was co-transfected with 0.25 μg wild-type and 0.25 μg mutant plasmid. All groups of cells were co-transfected with plasmid containing KCNE1 cDNA. The total amount of all DNA was the same in all experiments. Cells were incubated for 24 hr and then seeded for electrophysiological recordings, which were performed 48-54 hr after transfection.

For fluorescent microscopy, cells were transiently transfected with plasmid pcDNA6-V5-HisA/hKCNE1-hKCNQ1 using Metafectene PRO (Biontex, Germany) according to manufacturer recommendations. Cells were seeded on glass coverslips in 35 mm plates 24 hr before transfection. Plasmid DNA was mixed with Metafectene PRO (1:2) and transient transfection was performed when the cells were at 50% confluence. Cells were incubated in a complete medium without antibiotics for 48 hr, then fixed for immunostaining.

Fluorescent microscopy

48 hr after the transfection, cells were fixed with 1.5% paraformaldehyde, permeabilized with 0.1% triton X-100 in PBS, blocked with 1% BSA in PBST, and stained with anti-V5-tag primary antibodies (Bio-Rad, USA). Second antibodies used were donkey anti-mouse alexa 488 conjugated antibodies (Abcam, USA). Nuclei were stained with DAPI.

To quantify the ion channel expression in the membrane and cytoplasm, the intensity profile across the width of the cell was generated. This profile was segmented into 3 different sections: approximately 15% at each end of the cell profile, corresponding to the plasma membrane (M1 and M2, as shown in Figure 2b, lower graphs), and the remaining intermediate 70% of the surface plot, corresponding to the cytoplasmic compartments. For each of these areas in each cell, the Kv7.1 fluorescence intensity values were averaged and normalized to the average cell fluorescence intensity signal ($p<0.05$ for membrane versus cytosol, paired Student's t-test).

Immunoblotting

Mutant protein expression was analyzed by SDS-PAGE and immunoblotting with anti-1D4 and anti-V5 antibodies. The expression level was estimated using ImageLab software (BioRad, USA).

Electrophysiology

CHO-K1 cells on a small coverslip were placed in an experimental chamber with a constant flow of physiological solution of the following composition (mmol/L): 150 NaCl, 5.4 KCl, 1.8 CaCl2, 1.2 $MgCl_2$, 10 glucose, 10 HEPES, pH adjusted to 7.4 with NaOH, placed on the stage of an Eclipse Ti-S (Nikon, Japan) inverted fluorescence microscope. Currents were recorded at room temperature (24±0.5°C) using an Axopatch 200B amplifier (Molecular Devices, CA, USA). Only cells emitting green fluorescent light when irradiated with 480 nm excitation light were selected for recording. Patch pipettes of 1.5-2.5 MOhm resistance were made of borosilicate glass (Sutter Instrument, CA, USA) and filled with the following solution (mmol/L): 140 KCl, 1 $MgCl_2$, 5 EGTA, 4 MgATP, 0.3 Na_2GTP, 10 HEPES;

Preprints (www.preprints.org) | NOT PEER-REVIEWED | Posted: 14 June 2022 doi:10.20944/preprints202206.0199.v1

pH was adjusted to 7.2 with KOH. Series resistance and pipette and cell capacitances were compensated before the start of each recording.

Current amplitudes were normalized to the capacitive cell size (pA/pF). The voltage dependence of activation (evaluated from normalized tail current amplitudes) was fitted with a Boltzmann equation, y= Imax / (1 + exp((V0.5-V)/k)), to determine the membrane potential for half-maximal activation (V0.5) and the slope factor (k). Time courses of activation and deactivation were fitted with a single exponential function to obtain the time constants of activation (Ta) and deactivation (TD).

Computer simulations of human ventricular action potential

The ionic model of human ventricular action potential (AP) (epicardial version) TP2006 (Ten Tusscher and Panfilov 2006) was used to assess the effect of the K422E mutation on the AP waveform. This model includes parameters of all major ionic currents of a human ventricular myocyte: fast Na^+ current INa, L-type Ca^{2+} current with fast and slow voltage inactivation, background inward rectifier K^+ current I_{K1}, transient outward current Ito, rapid delayed rectifier K^+ current I_{Kr}, slow delayed rectifier K^+ current I_{Ks}, Na^+/Ca^{2+} exchanger current I_{NCX}, currents of Ca^{2+} and Na^+/K^+ pumps, background Na^+ and Ca^{2+} currents. Intracellular calcium dynamics is represented by a single-compartment sarcoplasmic reticulum, Ca^{2+}-induced Ca^{2+} release is described with a Markov-state model for the ryanodine receptor.

To simulate the experimental traces of IKs activation and tail currents, the following IKs parameters of the original model were updated: maximum conductivity (gKs), kinetic parameters V50 and slope. The fitting of these parameters was carried out by the least-squares method. In the original TP2006 model, gKs was 0.392 mS/µF, V50 was -5 mV, and slope was 14 mV [17]. Here, the values of gKs, V50 and slope in the control model (WT Kv7.1) were changed to fit our observed data.

The CVODE solver [31] and the Myokit software package [32] were used to solve the equations of the ionic model. The stimulation frequency was 1 Hz, the AP signals were recorded after reaching a steady state. To reach the steady-state, 100 APs were calculated. The following characteristics of the simulated AP were measured: AP duration at 50% (APD50) or 90% (APD90) repolarization, AP amplitude (APA) and resting membrane potential (RMP).

Statistics

The results are represented as means ± s.e.m. Normality of distribution and equality of variances were checked, and necessary transformation of variables (see above) were made before statistical testing. The density of tail IKs in different groups of cells at different levels of membrane potential were compared using two-way ANOVA with Tukey's multiple comparisons test. The parameters of the steady-state activation curve, kinetics of current activation and tail current deactivation were compared using the non-paired t-test. P values of < 0.05 were considered statistically significant.

Electrostatics

The protein electrostatic potential was generated with the PME electrostatics plugin (PMEPot) using 144 × 144 × 128 grid position counts (~1 Å spacing) [33]. PQR files were prepared with the use of the PDB2PQR web service [34].

Supplementary Materials: The following supporting information can be downloaded at: www.mdpi.com/xxx/s1, Figure S1: Simulated action potential (left panel) and IKs current (right panel) in control (WT) and heterozygote (WT/K422E) mutation models; Figure S2: Fragment of KCNQ1-CaM complex; Table S1: The parameters of IKs activation curve in CHO-K1 cells of WT, K422E/K422E and WT/K422Et groups; Table S2: Characteristics of simulated action potential in control and heterozygote WT/K422E mutation models.

Author Contributions: Conceptualization, O.S.S. and E.Z.; methodology, M.K., D.V.A. and G.L.; software, T.N.; formal analysis, V.N., T.N.; investigation, E.Z., M.K., K.B.P.; writing—original draft preparation, O.S.S., M.K.; writing—review and editing, G.L, D.V.A., E.Z.; visualization, M.K.;

supervision, E.Z.; funding acquisition, O.S.S. All authors have read and agreed to the published version of the manuscript.

Funding: This study was funded by Russian Science Foundation (22-14-00088 to O.S.S.).

Institutional Review Board Statement: Clinical and genetic evaluation was performed in accordance with the principles of the Declaration of Helsinki.

Informed Consent Statement: Informed consent was obtained from all adult subjects involved in the study.

Acknowledgments: Authors thank Lisa Trifonova for proof-reading the manuscript. G.L. would like to acknowledge the CNRS International Emerging Action (IEA) PRC RUSSIE 2019 (PRC no. 2773).

Conflicts of Interest: The authors declare no conflict of interest

References

1. Rahm A.K., Lugenbiel P., Schweizer P.A., Katus H.A., Thomas D. Role of ion channels in heart failure and channelopathies. *Biophys Rev*. **2018,** *10(4),* 1097-1106. doi: 10.1007/s12551-018-0442-3.
2. Ledford H.A., Ren L., Thai P.N., Park S., Timofeyev V., Sirish P., Xu W., Emigh A.M., Priest J.R., Perez M.V., Ashley E.A., Yarov-Yarovoy V., Yamoah E.N., Zhang X.D., Chiamvimonvat N. Disruption of protein quality control of the human ether-à-go-go related gene K+ channel results in profound long QT syndrome. *Heart Rhythm*. **2022** *19(2)*, 281-292. doi: 10.1016/j.hrthm.2021.10.005.
3. Wu X., Larsson H.P. Insights into Cardiac IKs (KCNQ1/KCNE1) Channels Regulation. *Int J Mol Sci*. 2020, *21(24)*, 9440. doi: 10.3390/ijms21249440.
4. Reilly L., Eckhardt L.L. Cardiac potassium inward rectifier Kir2: Review of structure, regulation, pharmacology, and arrhythmogenesis. *Heart Rhythm*. **2021**, *18(8),* 1423-1434. doi: 10.1016/j.hrthm.2021.04.008.
5. Medeiros-Domingo A., Tan B.-H., Crotti L., Tester D. J., Eckhardt L., Cuoretti A., Kroboth S. L., Song C., Zhou Q., Kopp D., Schwartz P. J., Makielski J. C., Ackerman M. J. Gain-of-function mutation S422L in the KCNJ8-encoded cardiac K(ATP) channel Kir6.1 as a pathogenic substrate for J-wave syndromes. *Heart Rhythm*, **2010**, *7*, 1466-1471,
6. Ohno S., Ozawa J., Fukuyama M., Makiyama T., Horie M. An NGS-based genotyping in LQTS; minor genes are no longer minor. *J Hum Genet*. **2020**, *65(12)*, 1083-1091. doi: 10.1038/s10038-020-0805-z.
7. Amin A.S., Tan H.L., and Wilde A.A.M. Cardiac Ion Channels in Health and Disease. *Heart Rhythm*, **2010**, *7(1),* 117–26.
8. Long S.B., Campbell E.B. and Mackinnon R. Crystal Structure of a Mammalian Voltage-Dependent Shaker Family K+ Channel. *Science*, **2005**, *309(5736)*, 897–903.
9. Sokolova O., Accardi A., Gutierrez D., Lau A., Rigney M., and Grigorieff, N. Conformational Changes in the C Terminus of Shaker K+ Channel Bound to the Rat Kvbeta2-Subunit. *Proceedings of the National Academy of Sciences of the United States of America*, **2003**, *100,* 12607–12.
10. Sun J. and MacKinnon R. Structural Basis of Human KCNQ1 Modulation and Gating. *Cell*, **2020,** *180(2),* 340-347.e9.
11. Kimoto K., Kinoshita K., Yokoyama T., Hata Y., Komatsu T., Tsushima T., Nishide K., Yamaguchi Y., Mizumaki K., Tabata T., Inoue H., Nishida N., and Fukurotani K. Characterization of a Novel Mutant KCNQ1 Channel Subunit Lacking a Large Part of the C-Terminal Domain. *Biochemical and Biophysical Research Communications,* **2013**, *440(2),* 283–88.
12. Pischalnikova A.V. and Sokolova O.S. The Domain and Conformational Organization in Potassium Voltage-Gated Ion Channels. *Journal of Neuroimmune Pharmacology*, **2009,** *4*, 71–82.
13. Chang, A., Abderemane-Ali F., Hura G.L., Rossen N.D., Gate R.E., and Minor D.L. A Calmodulin C-Lobe Ca2+-Dependent Switch Governs Kv7 Channel Function. *Neuron,* **2018**, *97(4)*, 836.
14. Haitin, Y., Wiener R., Shaham D., Peretz A., Ben Tal Cohen E., Shamgar L., Pongs O., Hirsch J.A., and Attali B. Intracellular Domains Interactions and Gated Motions of I(KS) Potassium Channel Subunits. *The EMBO Journal*, **2009**, *28(14),* 1994–2005.
15. Aivar, P., Fernández-Orth J., Gomis-Perez C., Alberdi A., Alaimo A., Rodríguez M.S., Giraldez T., Miranda P., Areso P., and Villarroel A. Surface Expression and Subunit Specific Control of Steady Protein Levels by the Kv7.2 Helix A-B Linker. *PLoS ONE*, **2012,** *7(10),* 47263.
16. Sachyani, D., Dvir M., Strulovich R., Tria G., Tobelaim W., Peretz A., Pongs O., Svergun D., Attali B., and Hirsch J.A. Structural Basis of a Kv7.1 Potassium Channel Gating Module: Studies of the Intracellular c-Terminal Domain in Complex with Calmodulin. *Structure*, **2014**, *22(11),* 1582–94.
17. Ten Tusscher, K.H.W. J. and Panfilov A. V. Alternans and Spiral Breakup in a Human Ventricular Tissue Model. *American Journal of Physiology - Heart and Circulatory Physiology*, **2006**, *291(3),* 1088–1100.
18. Maleckar, M.M., Myklebust L., Uv J., Florvaag P.M., Strøm V., Glinge C., Jabbari R., Vejlstrup N., Engstrøm T., Ahtarovski K., Jespersen T., Tfelt-Hansen J., Naumova V., and Arevalo H. Combined In-Silico and Machine Learning Approaches Toward Predicting Arrhythmic Risk in Post-Infarction Patients. *Frontiers in Physiology*, **2021**, *12*.

19. Aizawa, Y., Ueda K., Wu L.M., Inagaki N., Hayashi T., Takahashi M., Ohta M., Kawano S., Hirano Y., Yasunami M., Aizawa Y., Kimura A., and Hiraoka M. Truncated KCNQ1 Mutant, A178fs/105, Forms Hetero-Multimer Channel with Wild-Type Causing a Dominant-Negative Suppression Due to Trafficking Defect. *FEBS Letters*, **2004**, *574(1–3),* 145–50.
20. Aromolaran, A.S., Subramanyam P., Chang D.D., Kobertz W.R., and Colecraft H.M. LQT1 Mutations in KCNQ1 C-Terminus Assembly Domain Suppress IKs Using Different Mechanisms. *Cardiovascular Research*, **2014**, *104(3),* 501–11.
21. Harmer, S.C., Mohal J.S., Royal A.A., McKenna W.J., Lambiase P.D., and Tinker A. Cellular Mechanisms Underlying the Increased Disease Severity Seen for Patients with Long QT Syndrome Caused by Compound Mutations in KCNQ1. *The Biochemical Journal,* **2014**, *462(1),* 133–42.
22. Splawski I, Shen J, Timothy KW, Lehmann MH, Priori S, Robinson JL, Moss AJ, Schwartz PJ, Towbin JA, Vincent GM, Keating MT. Spectrum of Mutations in Long-QT Syndrome Genes. *Circulation*, **2000**, *102(10),*1178–85.
23. Choveau FS, Abderemane-Ali F, Coyan FC, Es-Salah-Lamoureux Z, Baro I, Loussouarn G. Opposite Effects of the S4-S5 Linker and PIP(2) on Voltage-Gated Channel Function: KCNQ1/KCNE1 and Other Channels. *Frontiers in Pharmacology*, **2012**, *3*.
24. Choveau FS, Rodriguez N, Ali FA, Labro AJ, Rose T, Dahimène S, Boudin H, Le Hénaff C, Escande D, Snyders DJ, Charpentier F. KCNQ1 Channels Voltage Dependence through a Voltage-Dependent Binding of the S4-S5 Linker to the Pore Domain. *The Journal of Biological Chemistry*, **2011**, *286(1),* 707.
25. Malak, O.A., Gluhov G.S., Grizel A.V., Kudryashova K.S., Sokolova O.S., and Loussouarn G. Voltage-Dependent Activation in EAG Channels Follows a Ligand-Receptor Rather than a Mechanical-Lever Mechanism. *The Journal of Biological Chemistry,* **2019**, *294(16),* 6506.
26. Malak O.A., Es-Salah-Lamoureux Z., and Loussouarn G. HERG S4-S5 Linker Acts as a Voltage-Dependent Ligand That Binds to the Activation Gate and Locks It in a Closed State. *Scientific Reports*, **2017**, *7(1).*
27. Richards S, Aziz N, Bale S, Bick D, Das S, Gastier-Foster J, Grody WW, Hegde M, Lyon E, Spector E, Voelkerding K. Standards and Guidelines for the Interpretation of Sequence Variants: A Joint Consensus Recommendation of the American College of Medical Genetics and Genomics and the Association for Molecular Pathology. *Genetics in Medicine : Official Journal of the American College of Medical Genetics*, **2015**, *17(5),* 405.
28. Veerman CC, Verkerk AO, Blom MT, Klemens CA, Langendijk PN, Van Ginneken AC, Wilders R, Tan HL. Slow Delayed Rectifier Potassium Current Blockade Contributes Importantly to Drug-Induced Long QT Syndrome. *Circulation: Arrhythmia and Electrophysiology,* **2013**, *6(5),* 1002–9.
29. Karlova M.G., Voskoboynikova N., Gluhov G. S., Abramochkin D., Malak O. A., Mulkidzhanyan A., Loussouarn G., Steinhoff H. J., Shaitan K. V., and Sokolova O. S. Detergent-Free Solubilization of Human Kv Channels Expressed in Mammalian Cells. *Chemistry and Physics of Lipids,* **2019**, *219*, 50–57.
30. Nicolas C.S., Park K.H., El Harchi A., Camonis J., Kass R.S., Escande D., Mérot J., Loussouarn G., Le Bouffant F., and Baró I.. 2008. IKs Response to Protein Kinase A-Dependent KCNQ1 Phosphorylation Requires Direct Interaction with Microtubules. *Cardiovascular Research*, **2008**, *79(3),* 427–35.
31. Hindmarsh A.C., Brown P.N., Grant K.E., Lee S.L., Serban R., Shumaker D.E., and Woodward C.S. SUNDIALS. *ACM Transactions on Mathematical Software*, **2005**, *31(3),* 363–96.
32. Clerx, M., Collins P., de Lange E., and Volders P.G.A. Myokit: A Simple Interface to Cardiac Cellular Electrophysiology. *Progress in Biophysics and Molecular Biology*, **2016**, *120(1–3),* 100–114.
33. Aksimentiev A. and Schulten K. Imaging α-Hemolysin with Molecular Dynamics: Ionic Conductance, Osmotic Permeability, and the Electrostatic Potential Map. *Biophysical Journal*, **2005**, *88(6),* 3745–61.
34. Jurrus E, Engel D, Star K, Monson K, Brandi J, Felberg LE, Brookes DH, Wilson L, Chen J, Liles K, Chun M. Improvements to the APBS Biomolecular Solvation Software Suite. *Protein Science,* **2018**, *27(1)*, 112–28.